Stability of a boost converter fed from photovoltaic source

Abdullah Abusorrah [a], Mohammed M. Al-Hindawi [a], Yusuf Al-Turki [a], Kuntal Mandal [b,a,*],
Damian Giaouris [c], Soumitro Banerjee [b,a], Spyros Voutetakis [c], Simira Papadopoulou [c,d]

[a] *Department of Electrical and Computer Engineering, College of Engineering, King Abdulaziz University, Jeddah, Saudi Arabia*
[b] *Department of Physical Sciences, Indian Institute of Science Education & Research – Kolkata, Mohanpur Campus, 741252 West Bengal, India*
[c] *Centre for Research and Technology Hellas, Chemical Process and Energy Resources Institute, Thessaloniki, Greece*
[d] *Department of Automation Engineering, Alexander Technological Educational Institute of Thessaloniki, Greece*

Abstract

The use of photovoltaic panels has become very attractive in distributed power generation systems as they provide a clean and cheap form of energy. There are various converter topologies that are employed in order to connect these sources to the grid but almost always the main component is a DC–DC converter. Most readily available DC–DC converters are designed to work under a (nearly) constant voltage source and therefore their behaviors may not be as expected when connected to a variable current source like a photovoltaic panel. In fact, as it is reported in this paper, the behavior of the overall system (PV panel/DC–DC converter) can be drastically different from the desired one which may have a detrimental effect on the grid. As a case study, this paper explores the dynamics and stability of a boost converter that is fed from a photovoltaic panel under an ohmic load. All major control methods (peak/average current mode control, voltage mode control) are considered. We show with numerical, experimental and analytical results that the converter can behave unpredictably (or chaotically) when the output of the PV varies in response to the variation in solar radiation, and we report for the first time how the domain of stability in the parameter-space and the mechanisms of instability are affected by the characteristics of the photovoltaic source. The dynamical features are explored from circuit theory and nonlinear dynamics points of view. This knowledge will help in compensating for the aforementioned uncertainty and can be used to design converters that remain stable throughout the range of incident solar radiation and load values. The results have been experimentally validated.
© 2013 Elsevier Ltd. All rights reserved.

Keywords: Photovoltaics; DC–DC converter; Fast-scale instability; Subharmonic oscillation; Switching control

1. Introduction

With the depletion of fossil fuels, the utilization of renewable sources is assuming great importance. One of the most promising renewable sources is solar energy converted to electrical energy through photovoltaic means (Agrawal, 2012; Battisti and Corrado, 2005). In countries like Saudi Arabia and India, solar energy is available in abundance, and constitutes a promising solution of the energy problem in the future (Bull, 2001; Suri et al., 2007; Solangi et al., 2011).

However, the power available from such a photovoltaic source is variable in nature. The voltage, the current, and consequently the power continuously vary depending on the incident solar energy, and the load. Naturally, some power processing unit has to be placed between the source and the load (Xiao et al., 2007). If the load is a DC power consumer or a battery, a simple DC–DC converter can be used as the interface. Normally, a boost converter is favored for this purpose because of its continuous input current characteristics (Jain and Agarwal, 2007;

---

* Corresponding author at: Department of Physical Sciences, Indian Institute of Science Education & Research – Kolkata, Mohanpur Campus, 741252 West Bengal, India. Tel.: +91 9830952246.

E-mail address: kmandal1980@gmail.com (K. Mandal).

Abouobaida and Cherkaoui, 2011; Taghvaee et al., 2012; Farahat et al., 2012).

However, the boost converters available off-the-shelf are designed to operate with a voltage source, and the useful range of the external parameters (like the input voltage and the load) are defined based on the range of a stable periodic operation. The extremities of the useful range are generally delimited by the instabilities or "bifurcations" that can greatly increase the current ripple and therefore damage the converter, the supply source and the load. These instabilities have attracted a lot of interest in the past and a lot of work has been done in order to understand the mechanism behind them that forces the converter to be unstable and to operate with high current/voltage ripple (Banerjee and Verghese, 2001; Tse, 2003). More specifically, these bifurcations can create another stable operating mode (saddle-node bifurcation) in an undesirable area, can impose a slow sine wave on the system's response (slow-scale bifurcation) or, most commonly, can increase the current ripple (fast-scale bifurcation). As it has been reported in (Banerjee and Verghese, 2001), it is also possible to have a so-called nonsmooth bifurcation (called border collision) that effectively can completely change the behavior of the converter and can abruptly lead to chaotic behavior.

When these converters are used in distributed energy applications that employ PV panels, the operating conditions can be vastly different than in the aforementioned studies and hence there is a great need for new work that focuses specifically in such systems. First of all, the converter is not fed by a (nearly) constant voltage source but from a variable current source that can vary from full power (during the noon) to zero (during the night). The load can also greatly change depending on the application. Finally, the interactions of these converters within the overall (micro) grid are far more significant than those in a simple domestic application (like a laptop). Unfortunately very little work has been done that focuses on the bifurcation behavior of the combined system (PV panel/DC–DC converter) and where it is done, the work is mainly based on simplified models of the converter and the PV panel (Maeda and Saito, 2010; Xiong et al., 2012, 2013). This is exactly the purpose and the novel contribution of this paper, i.e., to study the nonlinear behavior of the combined system under various levels of solar irradiation and loading conditions using the exact switched model of the converter and the actual V–I characteristics of the PV panel. This study is supported by numerical, experimental and analytical results.

It has to be noted here that in such systems various maximum power point trackers (Salas et al., 2006; Esram and Chapman, 2007; Wujian and Qiuhua, 2008; Enrique et al., 2007) are employed to extract the maximum possible power from the PV panels. Where the objective of the controller is to obtain maximum power, we just assume that such an algorithm is in operation which keeps the operation close to the maximum power point. Thus, in this paper, we avoid the dynamical features caused by the

instabilities in the maximum power point tracing algorithms (Hohm and Ropp, 2003; Zegaoui et al., 2011) and concentrate on the dynamical features caused by the interaction between the nonlinear character of the photovoltaic source with that of the power converter. More specifically, we study various control strategies that are normally employed to control the switching of the power converter. Prominent among these are (a) the peak current mode control, (b) the average current mode control, and (c) the voltage mode control.

The paper is organized as follows. The characteristics of the photovoltaic source and the boost converter are given in Section 2. Section 3 presents the simulation results under different control methods which include the peak current mode control, average current mode control, voltage mode control, and maximum power point tracking control. In Section 4, the experimental results are presented which include peak current mode control, average current mode control, and maximum power point tracking control. Section 5 concludes the work.

2. System description

2.1. Characteristics of the photovoltaic source

The photovoltaic source is basically a current source, whose value is dependent on the incident solar radiation (called *insolation*). This is called the photo-current, I_{ph}. The whole cell is nothing but a P–N junction, and hence acts like a diode. The electron–hole pairs created by the incident solar radiation are separated by the P–N junction, and the electrons move to the N-side and the holes to the P-side. These are collected by electrodes. There will be some resistance in the path of the electrons and holes, called R_s, which will be in series with the circuit. Some of the electrons and holes recombine before reaching the electrodes. This has the effect of "shunting" a part of the current, and so the equivalent resistance R_{sh} is in parallel to the circuit. Thus the equivalent circuit (Villalva et al., 2009; Siddiqui et al., 2013) of the solar cell is as given in Fig. 1. When a number of cells are connected to form a solar panel, in a "lumped" model it can be assumed to be represented by the same equivalent circuit, only with different parameter values to represent the characteristics of a panel.

The diode equation is

$$i_D = I_0\big(e^{Av_D} - 1\big)$$
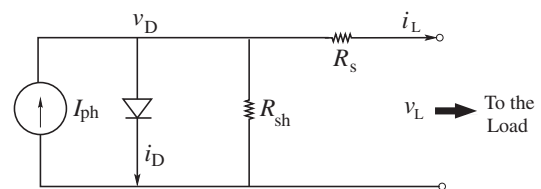
Fig. 1. Equivalent circuit of a solar panel.

where $A = \frac{q}{\gamma k T_e}$, and I_o is the saturation current of the diode, q is the charge of an electron $= 1.6 \times 10^{-19}$ coulombs, k is the Boltzmann's constant $= 1.38 \times 10^{-23}$ J/K, T_e is the absolute temperature, and γ is the diode ideality factor.

The current balance equation is

$$I_{ph} - i_D - i_{sh} = i_L$$

or

$$I_{ph} - I_0 \left(e^{A v_D} - 1 \right) - \frac{v_D}{R_{sh}} = i_L$$

Now, since

$$v_D = v_L + i_L R_s,$$

we get

$$I_{ph} - I_0 \left(e^{A(v_L + i_L R_s)} - 1 \right) - \frac{v_L + i_L R_s}{R_{sh}} = i_L \tag{1}$$

This is the basic equation of the solar panel, which is transcendental. It can be solved numerically using the Newton–Raphson algorithm, to give the v–i characteristics of the solar panel (Fig. 2). We assume the parameter values $I_{ph} = 1$ A, $I_o = 10^{-11}$ A, $\gamma = 10$, $R_s = 0.1\ \Omega$, $R_{sh} = 100\ \Omega$, and $T_e = 300$ K.

I_{sc} is the value of i_L when the load is short-circuited, and V_{oc} is the value of v_L when the load is open circuited. The panel gives maximum output power at the knee point, i.e., at a specific combination of output voltage and current. One of the desirable characteristics of the load is to be able to operate close to this maximum power point (MPP).

2.2. Characteristics of the boost converter

The power produced by the PV panel has to be processed before delivering to the load, and the boost converter is a basic DC–DC converter that is often used for that purpose. When the boost converter (with a resistive load) is supplied from to the PV panel, the full equivalent circuit becomes as shown in Fig. 3. The state variables are i_L and v_o.

When the switch is turned ON, the inductor current rises and energy is stored in it. When the switch is turned OFF, the stored energy is delivered to the load. The inductor current falls, and the voltage across it adds to the applied voltage v_L to give the voltage across the load. It may be noted
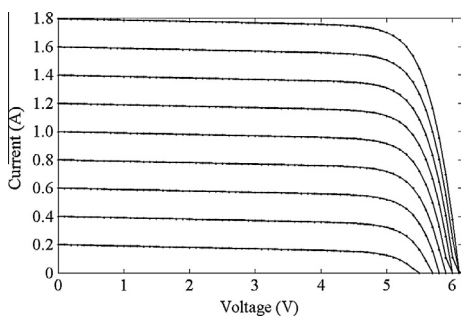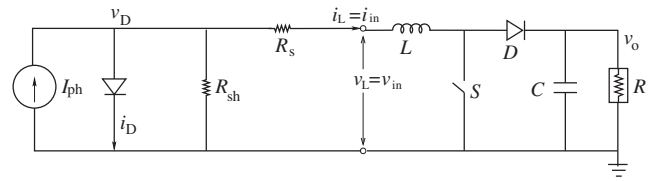
Fig. 3. The solar cell coupled with a boost converter.

that the input current is continuous (unlike the buck converter) – that is why this converter is suitable for operation with a current source. The circuit configuration during the ON period will be termed as subsystem M_1, and that during the OFF period as subsystem M_2.

When the switch S is turned ON (subsystem M_1), the state equations are

$$\frac{di_L}{dt} = \frac{v_L}{L} \tag{2}$$

$$\frac{dv_o}{dt} = -\frac{v_o}{RC} \tag{3}$$

When the switch is OFF (subsystem M_2), the state equations are

$$\frac{di_L}{dt} = \frac{v_L}{L} - \frac{v_o}{L} \tag{4}$$

$$\frac{dv_o}{dt} = \frac{i_L}{C} - \frac{v_o}{CR} \tag{5}$$

These are solved by the Runge–Kutta algorithm to obtain the evolution of the state variables. There is one complication, however. When the converter is connected to the PV panel, the input voltage is not constant, and depends on the instantaneous value of the current drawn. So, at each Runge–Kutta step, the value of V_L is obtained from the v–i characteristics of the panel before proceeding to the next step. This aspect changes the dynamics and stability of the converter, which is the focus of the present investigation.

2.3. Characteristics of nonlinear systems

As it is known, the desired operation of a DC–DC converter is an oscillatory motion around a predefined value, with the same rate as the driving clock. This periodic operation is called period-1 mode and the PV-fed boost converter, under different control methods, must always be designed to operate under this type of operation. Even though the period-1 is the desirable mode, it is not the only possibility and when this occurs a bifurcation has taken place that can greatly reduce the system's performance.

In order to quantify the stability of the period-1 motion (and hence the robustness of our system), the equations of the system are linearized around the desired orbit and from the eigenvalues of the resulted Jacobian we can determine how close we are to a bifurcation (Banerjee and Verghese, 2001; Tse, 2003). If the moduli of the eigenvalues are inside the unit circle the periodic motion is stable; in the opposite

Fig. 2. The v–i characteristics of a solar panel.

case we can have three different scenarios: (a) one eigen-value is approaching -1 and this is the sign for a fast-scale bifurcation, (b) one eigenvalue approaches $+1$ and a saddle-node bifurcation is imminent, (c) complex-conjugate eigenvalues cross the unit circle which implies that a slow-scale bifurcation takes place. This tool can be used to design robust systems by exploring a wide range of parameters, for example, as shown in Fig. 6, by selecting a wide range of pairs (I_{ph}, I_{ref}) we can immediately determine the stable areas in the parameter space. Therefore we can easily choose the appropriate parameters that guarantee a stable operation.

Another useful tool that gives a global perspective of the overall system's behavior, and can again be used for the appropriate design, is the bifurcation diagram. This diagram is one of the most useful ways for the presentation of different dynamical behaviors and changes in them with the variation of the parameters. Selecting a single state variable for observation (e.g., the sampled inductor current), the diagram records its steady-state behavior as a function of one of the system parameters (e.g., the reference current), over its range of interest. This is done by plotting the sampled values of the state variable for each value of the parameter. For a nonautonomous system, generally the sampling is done in synchronism with the clock frequency (i.e., at the start of the switching cycle). A normal period-1 orbit appears as a single point in the diagram corresponding to the parameter. Similarly, a period-2 orbit appears as 2 different points. But the quasiperiodic orbit and chaotic orbit appears as a mess of points. The bifurcation diagram thus shows a panoramic view of the stability status as a parameter is varied.

3. Simulation results

In this section the dynamics and stability of the PV-fed boost converter under different control methods is thoroughly investigated through bifurcation diagrams and regions of stability in the parameter-space. This can then be used for the proper design in order to guarantee a satisfactory performance.

3.1. The peak current mode control

For operating close to the maximum power point, the peak current mode control (Fig. 4) is generally employed. In this controller, the switch is turned on by a free-running clock, and is turned off when the current reaches a reference value I_{ref}. Any clock signal coming during the on period is ignored.

In such a system, there are a few "design" parameters like L, C, clock frequency, etc., and there are a few variable parameters like the incident solar radiation (embodied in I_{ph}), the load resistance R, and the reference current I_{ref}. Our objective is to study the stability of the system when these variable parameters change while the converter is in operation.
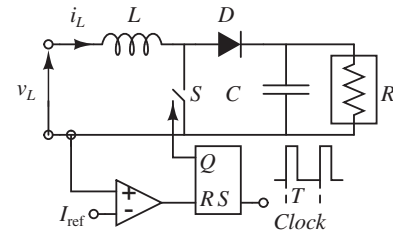
Fig. 4. Circuit diagram of the peak current mode controlled PV-fed boost converter.

It has been proposed to set the I_{ref} at the maximum power point (MPP). In that case, however, the ripple of the panel current occurs at one side of the MPP, and hence this strategy cannot extract maximum power out of the panel. Therefore the I_{ref} should be set above the MPP. To investigate this aspect, we study the dynamics and stability of the system as the value of I_{ref} is varied.

It is known (Deane, 1992; Chan and Tse, 1997) that, when such a converter is fed from a constant voltage source, when I_{ref} is increased the system undergoes a subharmonic instability (period doubling bifurcation) at a critical value of I_{ref} resulting in chaos. In order to check the effect of the photovoltaic panel characteristics on the system behavior, we increase I_{ref} in steps and obtain the bifurcation diagram (Fig. 5(a)).

It shows that the converter remains stable only if the I_{ref} is set at a low value, and loses stability for $I_{ref} > 1$ A (Table 1). Since the I_{MPP} ($= 1.3856$ A) would be above this value, it brings two desirable criteria in contradiction. For extracting a maximum power, the I_{ref} should be set such that the average inductor current is close to the maximum power point, i.e., $I_{ref} > I_{MPP}$. On the other hand, for maintaining stability, I_{ref} has to be below I_{MPP}. In general, the stability condition would demand precedence, and so the maximum power cannot be obtained from the solar panel.

This implies that the converter should be designed with the solar panel characteristics in mind, so that the above two criteria do not contradict each other. Any solar panel and converter will not satisfy this necessity.

Now we investigate the effect of the variation of incident solar radiation (Morel et al., 2011). The bifurcation diagram with I_{ph} as the variable parameter is given in Fig. 5(b). It shows that the converter is stable for low sunlight and becomes unstable for high values of sunlight (Table 2). This aspect, naturally, has to be taken into account when designing the converter, so that it remains stable for the whole expected range of I_{ph}.

The overall picture emerges when we look at the region of stability in the $I_{ph} - I_{ref}$ parameter space (Fig. 6).

It shows that for each value of the photo-current, the system is stable for a specific range of I_{ref}, and is unstable for a setting below or above this range. The stable range of I_{ref}, in turn, increases with the increase of I_{ph}, but not proportionally.

If I_{ph} is fixed at a certain value, the performance of the converter will depend upon the load, and may be unstable
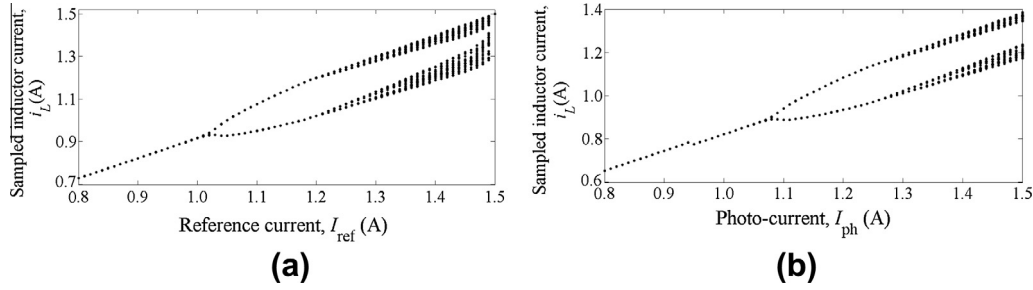
Fig. 5. The bifurcation diagrams of the PV-fed boost converter (a) with I_{ref} as the bifurcation parameter; I_{ph} fixed at 1.5 A; (b) with I_{ph} as the bifurcation parameter; the reference current I_{ref} is set at the MPP dynamically. The other parameters are $L = 3.125$ mH, $C = 20$ μF, $R = 20$ Ω, $T = 1/10000$ s.

Table 1
Eigenvalues with variation of the reference current I_{ref} corresponding to Fig. 5(a). The eigenvalues of the Jacobian matrix was calculated using the Filippov method (Giaouris et al., 2008).

I_{ref} (A)	Orbit	Subsystem sequence	Eigenvalues
0.8	Stable Period-1	M_1–M_2	−0.7447, 0.5744
1.0	Stable Period-1	M_1–M_2	−0.9903, 0.5813
1.01	Unstable Period-1	M_1–M_2	−1.0023, 0.5816
1.01	Stable Period-2	M_1–M_2; M_1–M_2	0.9991, 0.3612

Table 2
Eigenvalues with variation of photo-current I_{ph} corresponding to Fig. 5(b).

I_{ph} (A)	Orbit	Subsystem sequence	Eigenvalues
0.80	Stable Period-1	M_1–M_2	−0.8062, 0.5769
0.99	Stable Period-1	M_1–M_2	−0.9949, 0.5818
1.00	Unstable Period-1	M_1–M_2	−1.0067, 0.5820
1.00	Stable Period-2	M_1–M_2; M_1–M_2	0.9984, 0.3246
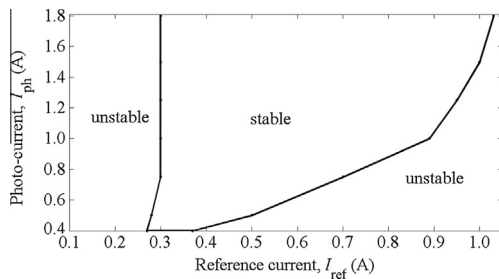
Fig. 6. The region of stability in the $I_{ph} - I_{ref}$ parameter space with $R = 20$ Ω.

at a critical value of the load resistance. In order to check this, we plot the bifurcation diagram with R as the variable parameter (Fig. 7(a)). It shows that, when the I_{ref} is set at MPP corresponding to the $I_{ph} = 1$ A, the converter is stable for low values of R, and becomes unstable when R exceeds about 22.4 Ω. The calculation of the eigenvalues (Table 3) shows that the system undergoes a fast-scale period doubling bifurcation, and subsequently becomes chaotic. Comparison with Fig. 7(b) shows that when the same converter

is fed from a constant voltage supply (corresponding to the MPP of the photovoltaic panel), the range of stability is slightly lower.

Our investigation revealed that the value of R at which the system loses stability depends on the incident solar radiation, i.e., on the value of I_{ph}. Fig. 8 shows the bifurcation curve in the $I_{ph} - R$ parameter space. It shows that for low values of I_{ph} the system is able to operate stably over a large range of load, but for high values of I_{ref} the available range of R becomes restricted.

3.2. Average current mode control

In the average current mode control (Fig. 9) the difference between the inductor current and the reference current is adjusted by the proportional-integral (PI) compensator to produce the control voltage:

$$v_{con} = K_p(I_{ref} - i_L) + K_i \int (I_{ref} - i_L)dt$$

This control voltage is compared with a ramp voltage

$$v_{ramp} = V_L + (V_U - V_L)\frac{t}{T}\text{mod}1$$

At the start of each clock cycle the switch is ON. When $v_{con} = v_{ramp}$, the switch is OFF for the rest of the cycle.

If I_{ph} is fixed at a certain value, the performance of the converter will depend upon the load, and it may become unstable at a critical value of the load resistance. In order to check this, we plot the bifurcation diagram with R as the variable parameter (Fig. 10(a)). It shows that, when the I_{ref} is set at maximum power point for $I_{ph} = 1$ A, the converter is stable for low values of R, and becomes unstable when R exceeds a critical value (for the chosen set of parameters, it is about 39.4 Ω). The calculation of the eigenvalues given in Table 4 shows that the system undergoes a fast-scale period doubling bifurcation, and subsequently becomes chaotic. When the same converter is fed from a constant voltage source (Fig. 10(b)), the bifurcation pattern remains the same, but the instability at a smaller value of the load resistance. This implies that the characteristics of the PV panel increases the range of stability of the converter.
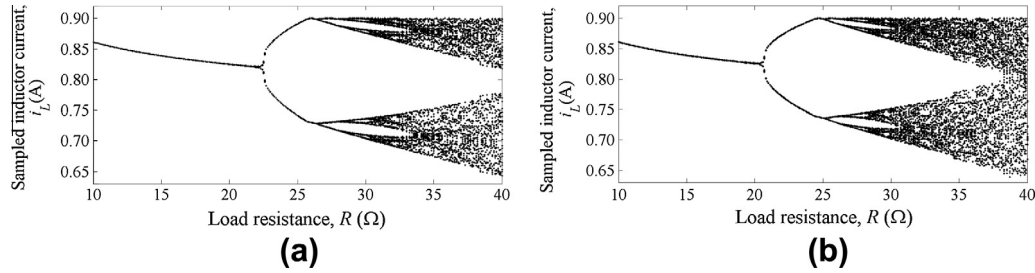
Fig. 7. Bifurcation diagrams with load resistance R as a varying parameter. The reference current I_{ref} is set at MPP corresponding to $I_{ph} = 1$ A. (a) Fed from photovoltaic panel where (b) fed from constant voltage $V_{in} = 5.1$ V which is set at the MPP for $I_{ph} = 1$ A.

Table 3
Eigenvalues with variation of load resistance R corresponding to Fig. 7(a).

R (Ω)	Orbit	Subsystem sequence	Eigenvalues
10.0	Stable Period-1	M_1–M_2	−0.4980, 0.2915
19.8	Stable Period-1	M_1–M_2	−0.9980, 0.5785
19.9	Unstable Period-1	M_1–M_2	−1.0024, 0.5803
19.9	Stable Period-2	M_1–M_2; M_1–M_2	0.9992, 0.4214
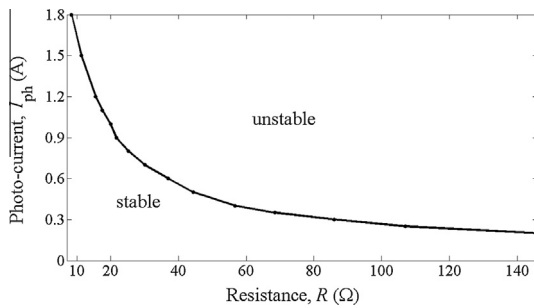
Fig. 8. The region of stability in the $I_{ph} - R$ parameter space.
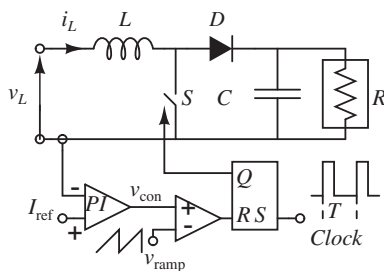
Fig. 9. Circuit diagram of the average current mode controlled PV-fed boost converter.

Now we investigate the effect of the variation of incident solar radiation. For each value of the incident solar radiation the reference current I_{ref} is set at the maximum power point. The bifurcation diagram with I_{ph} as the variable parameter is given in Fig. 11(a). It shows that the system loses stability at high values of the photo-current (Table 5). This indicates that when the solar intensity is high, the other parameters need to be adjusted to keep the converter stable. Such adjustable parameters are I_{ref}, K_p, and R.

Fig. 12 shows the parameter space plots of I_{ph} versus I_{ref}, I_{ph} versus R, K_p versus R, and I_{ph} versus K_p. These curves help in choosing the appropriate values of the internal parameters K_p and I_{ref} for given values of the external parameters I_{ph} and R.

3.3. Voltage mode control

In the voltage mode control (Fig. 13), the objective is to keep the output voltage constant. To achieve this, the difference between a constant reference voltage and the output voltage of the boost converter is adjusted by the proportional-integral (PI) compensator to produce the control voltage:

$$v_{con} = K_p(v_o - V_{ref}) + K_i \int (v_o - V_{ref})dt$$

At the start of each clock cycle the switch in ON. When $v_{con} = v_{ramp}$, the switch is OFF for the rest of the cycle.

Fig. 14 gives the stability status with the variation of the load resistance and the photo-current. It shows that the converter is stable for low values of both variables, and becomes unstable at some critical parameter values. But, even when the converter is stable, the operating point oscillates away from the maximum power point (see Figs. 15 and 16), and so the whole system becomes quite inefficient.

3.4. Maximum power point tracking control

In Sections 3.1 and 3.2, we have adopted the current mode control to achieve maximum power point tracking, by adjusting the I_{ref}. In Section 3.3 we have shown that the absence of maximum power point tracking makes the system very inefficient. There exists a method of maximum power point tracking (Bennett et al., 2012; Enrique et al., 2007) which is quite similar to voltage mode control, that is used more often in practice (Liu and Huang, 2011; Kalirasu and Dash, 2010). In this MPP-tracking control (Fig. 17) the difference between the reference voltage from maximum power point and the actual voltage of the photovoltaic cell is amplified by the proportional gain to produce the control voltage:

$$v_{con} = K_p(v_L - V_{ref})$$
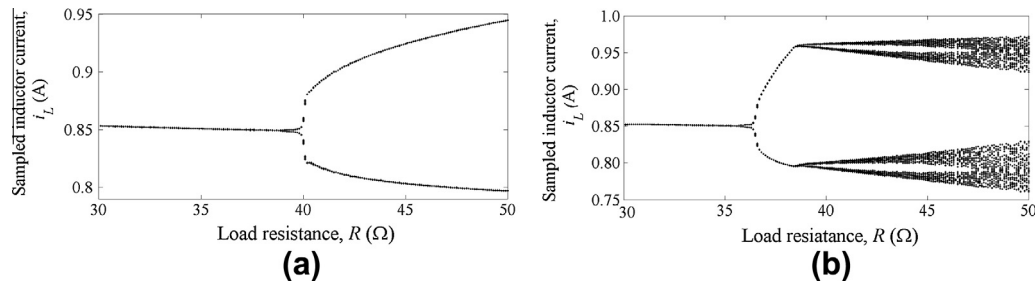
Fig. 10. Bifurcation diagrams with load resistance as the varying parameter. The other parameters are: $V_L = 0$, $V_U = 1$ V, $K_p = 20$, $K_i = 800$ s^{-1}, $I_{ref} = 0.9$ A. (a) Fed from photovoltaic panel (b) fed from constant voltage $V_{in} = 5.1$ V which is set at the MPP for $I_{ph} = 1$ A.

Table 4
Eigenvalues with variation of load resistance R corresponding to Fig. 10(a).

R (Ω)	Orbit	Subsystem sequence	Eigenvalues
30.0	Stable Period-1	M_1–M_2	−0.5772, 0.5635, 0.9961
39.4	Stable Period-1	M_1–M_2	−0.9990, 0.7048, 0.9961
39.5	Unstable Period-1	M_1–M_2	−1.0028, 0.7057, 0.9961
39.5	Stable Period-2	M_1–M_2; M_1–M_2	0.9981, 0.5003, 0.9920
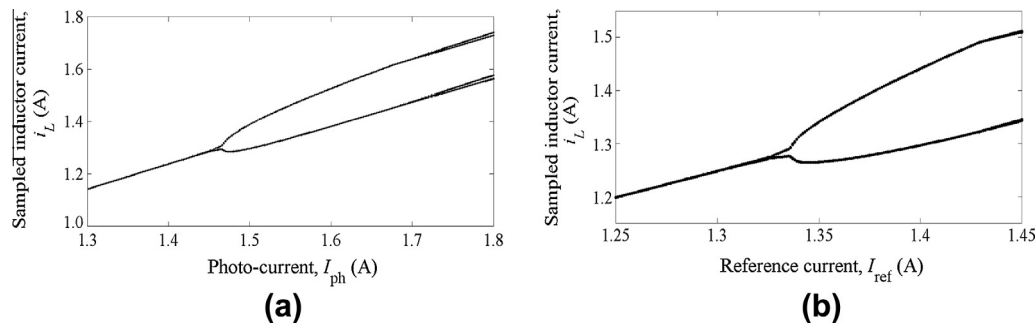
Fig. 11. Bifurcation diagrams with (a) photo-current as a varying parameter and the reference current is set dynamically at the MPP and (b) reference current as a varying parameter when $I_{ph} = 1.6$ A. The other parameters are: $V_L = 0$, $V_U = 1$ V, $K_p = 20$, $K_i = 800$ s^{-1}, $R = 25$ Ω.

Table 5
Eigenvalues with variation of photo-current I_{ph} corresponding to Fig. 11(a).

I_{ph} (A)	Orbit	Subsystem sequence	Eigenvalues
1.30	Stable Period-1	M_1–M_2	−0.8682, 0.6452, 0.9961
1.43	Stable Period-1	M_1–M_2	−0.9911, 0.6478, 0.9961
1.44	Unstable Period-1	M_1–M_2	−1.0002, 0.6480, 0.9961
1.44	Stable Period-2	M_1–M_2; M_1–M_2	0.9973, 0.2822, 0.9918

This control voltage is compared with a ramp voltage

$$v_{ramp} = V_L + (V_U - V_L)\frac{t}{T} \bmod 1$$

At the start of each clock cycle the switch in ON. When $v_{con} = v_{ramp}$, the switch is OFF for the rest of the cycle.

If I_{ph} is fixed at a certain value, the performance of the converter will depend upon the load, and may become unstable at a critical value of the load resistance. The bifurcation diagram with R as the variable parameter (Fig. 18(a)) shows that, when the V_{ref} is set at maximum

power point for $I_{ph} = 1$ A, the converter is stable for low values of R, and becomes unstable when R exceeds about 40 Ω.

Similarly, the bifurcation diagram with I_{ph} as variable parameter is given in Fig. 18(b). It shows that the system loses stability at high values of the photo-current.

4. Experimental results

An experimental system was fabricated and tested where the parameters of the power stage were the same as in the
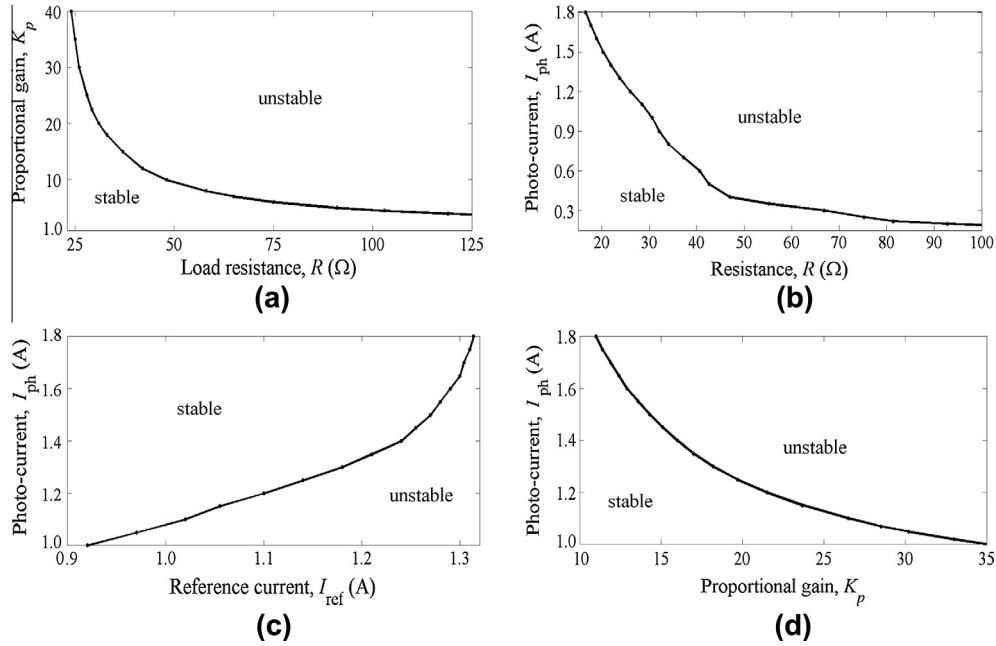
Fig. 12. The region of stability for the average current mode control of the PV-fed boost converter in the (a) $K_p - R$ parameter space with $I_{ph} = 1A$, (b) $I_{ph} - R$ parameter space with $K_p = 20$, (c) $I_{ph} - I_{ref}$ parameter space with $K_p = 20$, $R = 25\,\Omega$, and (d) $I_{ph} - K_p$ parameter space with $R = 25\,\Omega$ and the I_{ref} is set dynamically at the MPP for the given value of the I_{ph}.
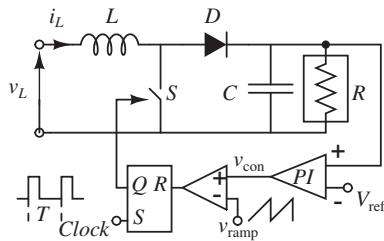
Fig. 13. Circuit diagram of the voltage mode controlled PV-fed boost converter.

simulation reported in the earlier sections. The input to the power stage was given from a photovoltaic panel with open circuit voltage 18.4 V and short circuit current 0.69 A at ambient sunlight condition. The parameters of the panel (Villalva et al., 2009) were calculated from the measured v–i characteristics of the panel as $R_s = 0.8\,\Omega$, $R_{sh} = 190\,\Omega$,

$I_o = 2.5 \times 10^{-7} A$ and $\gamma = 59.5$, and the temperature was $T_e = 295$ K.

4.1. Peak Current Mode (PCM) control

4.1.1. Varying reference current

To investigate the effect of the variation of reference current on the system performance, the experiment was conducted under constant light condition, with $I_{ph} = 0.5$ A. The load resistance is fixed at $R = 200\,\Omega$. It is noted that the output voltage of the converter is not constant for different load resistances.

At low value of the reference current the system is stable i.e., it gives the desirable period-1 waveform as shown in Fig. 19(a). But at higher values of the reference current it gives period-2 Fig. 19(b) and period-4 waveforms (Fig. 19(c)).
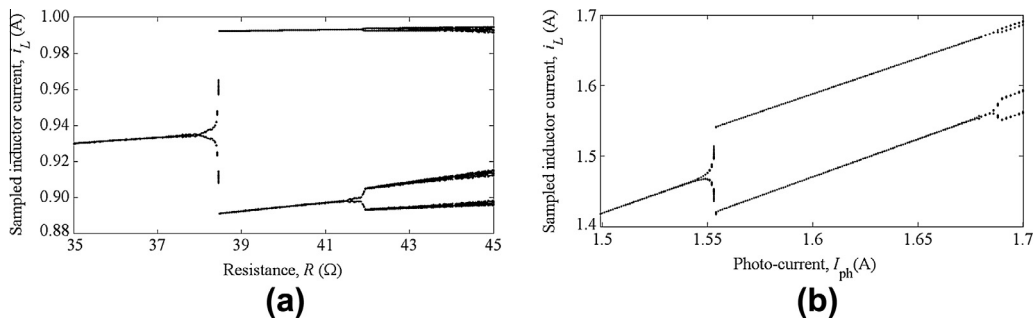
Fig. 14. Bifurcation diagrams (a) with load resistance as a varying parameter at $I_{ph} = 1$ A, and (b) with the photo-current as the varying parameter at $R = 20\,\Omega$. The other parameters are: $V_L = 0$, $V_U = 1$ V, $K_p = 1$, $K_i = 800\,\text{s}^{-1}$, $V_{ref} = 10$ V.
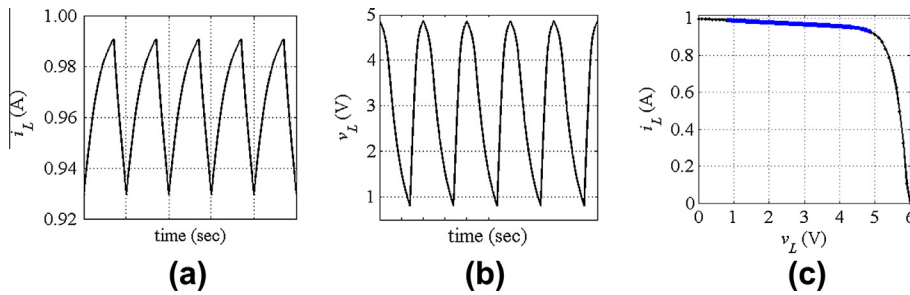
Fig. 15. The time-domain response of (a) photovolatic current (b) photovolatic voltage and (c) the variation of these two variables on the v–i characteristic of the panel corresponding to Fig. 14(a) at $R = 35\,\Omega$.
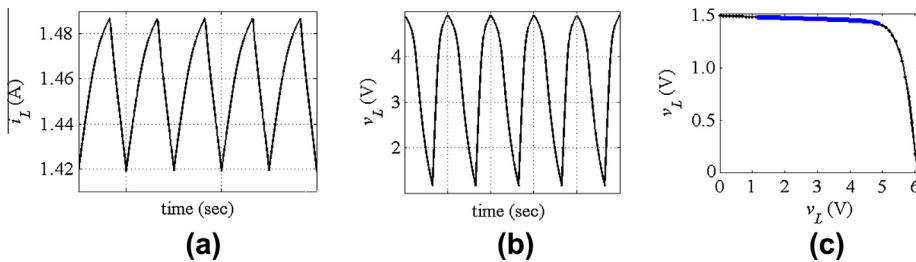
Fig. 16. The time-domain response of (a) photovolatic current (b) photovolatic voltage and (c) the variation of these two variables on the v–i characteristic of the panel corresponding to Fig. 14(b) at $I_{ph} = 1.5$ A.
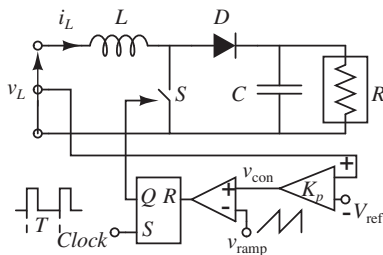
Fig. 17. Circuit diagram of the maximum power point tracking controlled PV-fed boost converter.

4.1.2. Varying load resistance

To see the effect of the load resistance on the system the photo-current is fixed at $I_{ph} = 0.5$ A. The open circuit voltage of the photovoltaic panel is 18.4 V. To get the maximum current from the photovoltaic panel the I_{ref} is fixed at 0.4 A.

Fig. 20(a) shows that the converter is stable for low values of R. With the increment of the R, the system

undergoes a period doubling bifurcation which is clear from Figs. 20(b) and 21.

4.2. Average Current Mode (ACM) control

In this control method we fixed $I_{ph} = 0.5$ A, $K_p = 20$, $V_L = 0$ V, $V_U = 1$ V.

4.2.1. Varying reference current

To see the effect of the variation of reference current on the system the load resistance is fixed at $R = 200\,\Omega$. At lower values of the reference current the system is stable (Fig. 22). When the value of the reference current is increased, the system goes to period-doubling bifurcation as shown in Fig. 23.

4.2.2. Varying load resistance

Similarly, to see the effect of the variation of load resistance on the system the reference current is fixed at
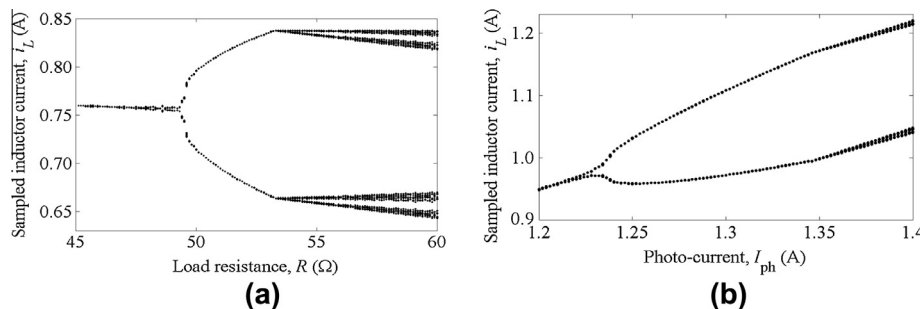
Fig. 18. Bifurcation diagrams with (a) the load resistance as a varying parameter at $I_{ph} = 1$ A, and (b) the photo-current as the varying parameter at $R = 40\,\Omega$. The other parameters are: $V_L = 0$, $V_U = 1$ V, $K_p = 5$, $V_{ref} = 5.1$ V.
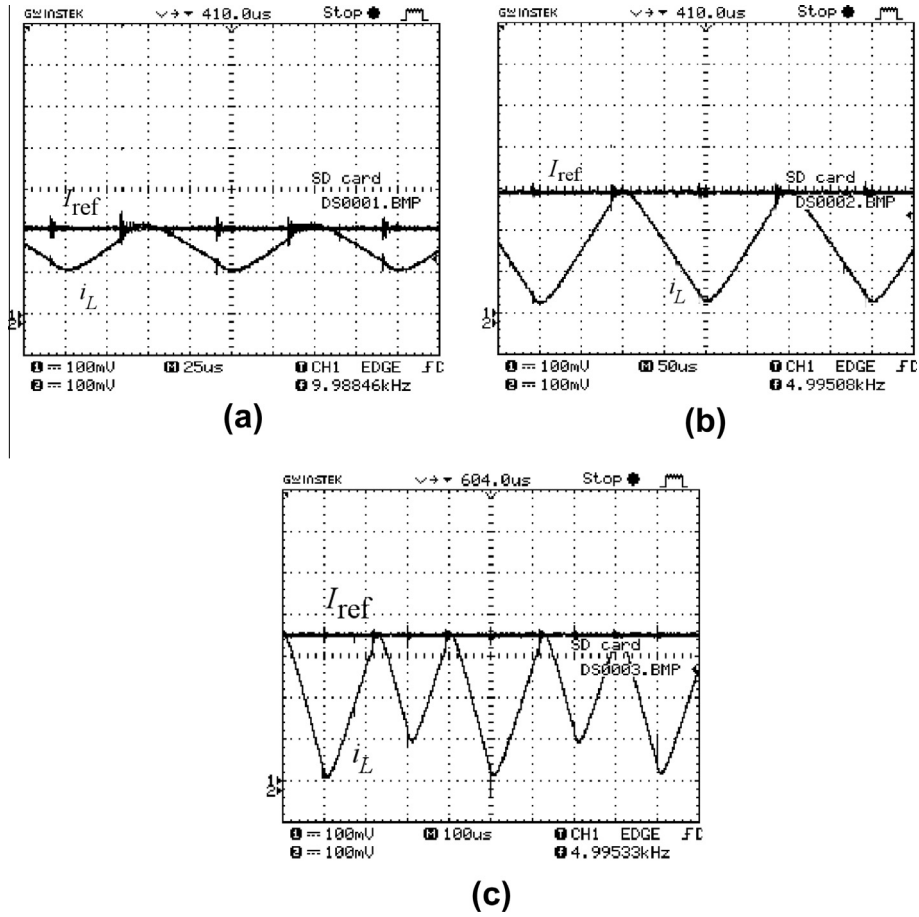
Fig. 19. The inductor current in PCM control with $R = 200\,\Omega$ (a) $I_{ref} = 0.2$ A, period-1 operation (b) $I_{ref} = 0.3$ A, period-2 operation, (c) $I_{ref} = 0.35$ A, period-4 operation. Note that the period of the first waveform is 100 μs, that of the second waveform is 200 μs, and that of the third is 400 μs. Each waveform is marked with 0.1 V/div.
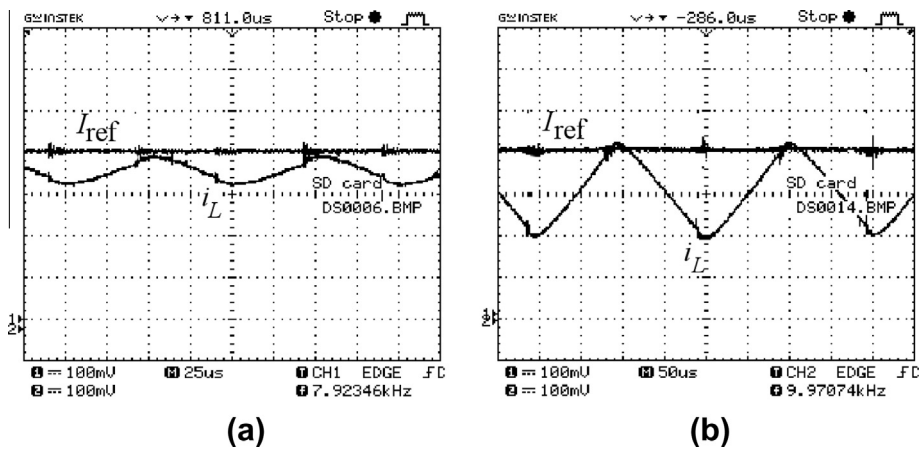
Fig. 20. Inductor current in PCM control with $I_{ref} = 0.4$ A, (a) $R = 80\,\Omega$, period-1 operation (b) $R = 120\,\Omega$, period-2 operation. The period of the first waveform is 100 μs and that of the second waveform is 200 μs. Each waveform is marked with 0.1 V/div.

$I_{ref} = 0.4$ A. At lower values of the resistance the system is stable (Fig. 24). When the value of the load resistance is increased, the system goes to period-doubling bifurcation as shown in Fig. 25.
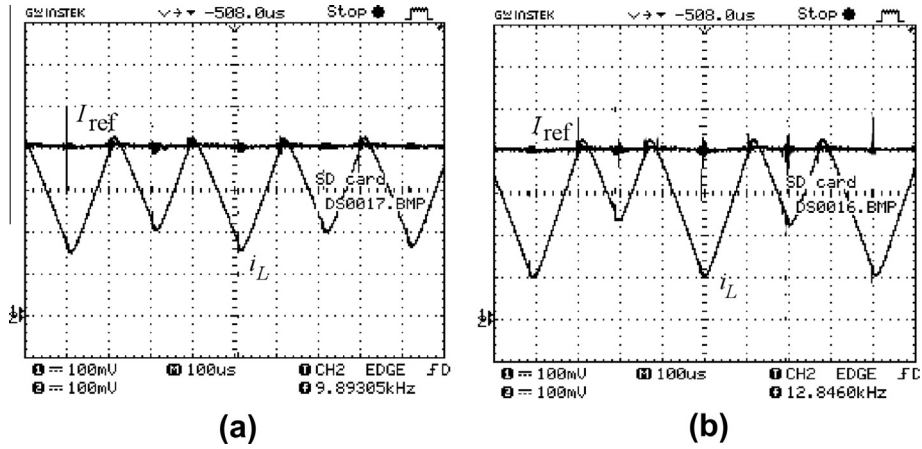
Fig. 21. Inductor current in PCM control with $I_{\text{ref}} = 0.4$ A (a) $R = 150\,\Omega$ (b) $R = 170\,\Omega$. Period-4 operation. The period of the waveforms is 400 μs, and each waveform is marked with 0.1 V/div.
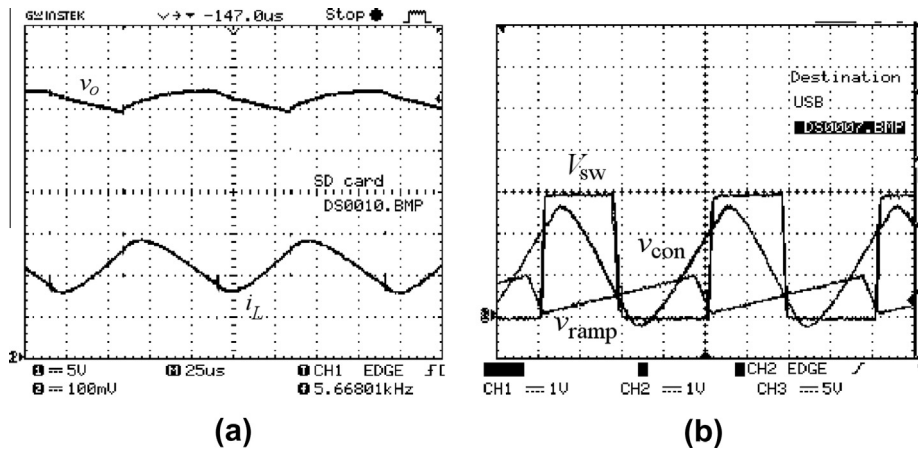
Fig. 22. ACM control with $I_{\text{ref}} = 0.3$ A (a) inductor current (0.1 V/div) and the output voltage (5 V/div) (b) switch signal. Period-1 operation. The period of the waveforms is 100 μs.
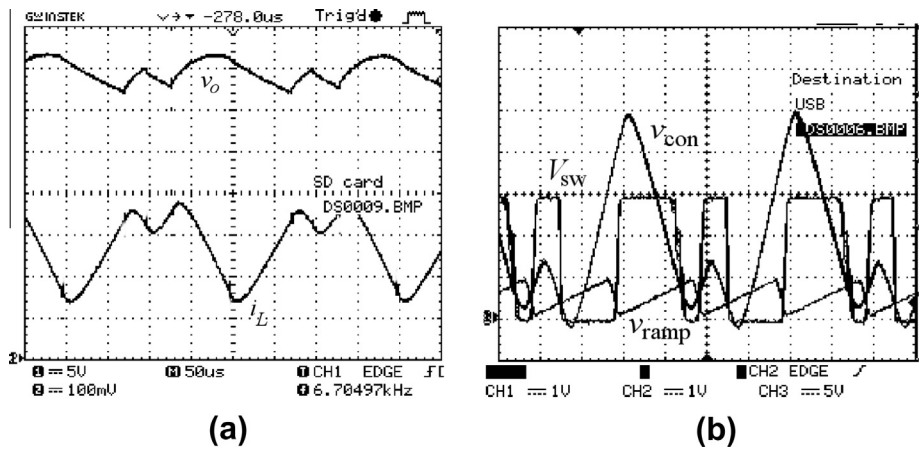
Fig. 23. ACM control with $I_{\text{ref}} = 0.4$ A (a) inductor current (0.1 V/div) and the output voltage (5 V/div) (b) switch signal. Period-2 operation. The period of the waveforms is 200 μs.
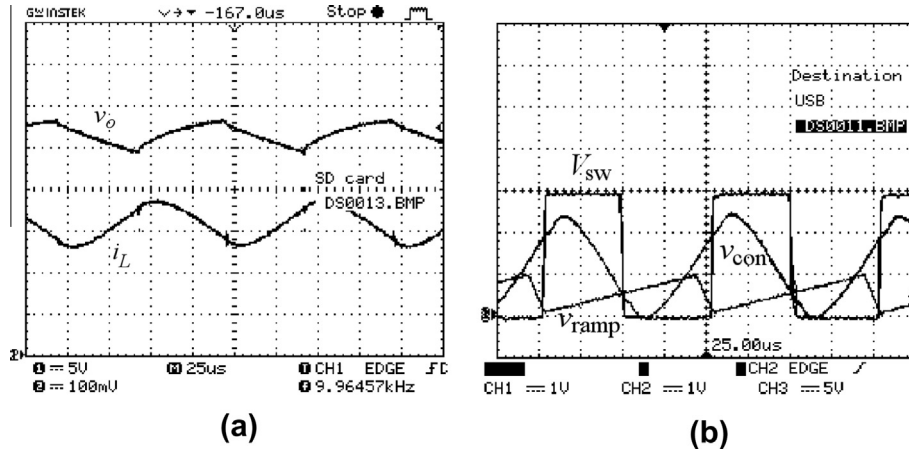
Fig. 24. ACM control with $R = 120\ \Omega$ (a) inductor current (0.1 V/div) and the output voltage (5 V/div) (b) switch signal. Period-1 operation. The period of the waveforms is 100 μs.
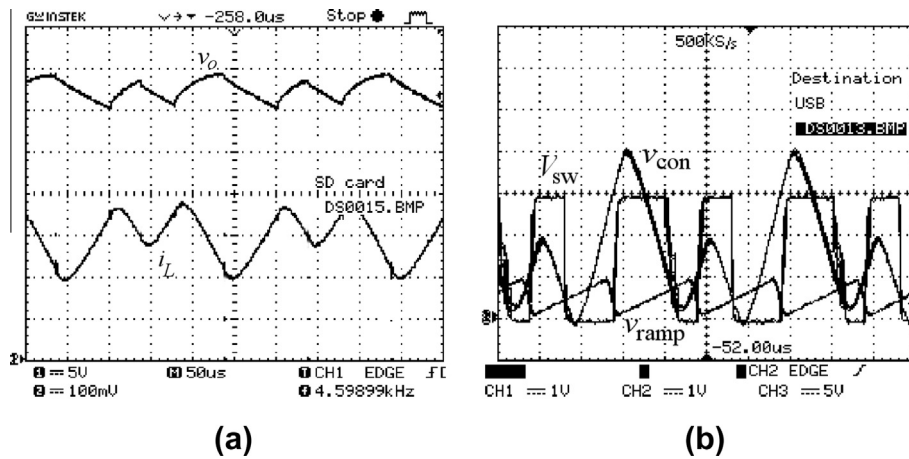
Fig. 25. ACM control with $R = 200\ \Omega$ (a) inductor current (0.1 V/div) and the output voltage (5 V/div) (b) switch signal. Period-2 operation. The period of the waveforms is 200 μs.
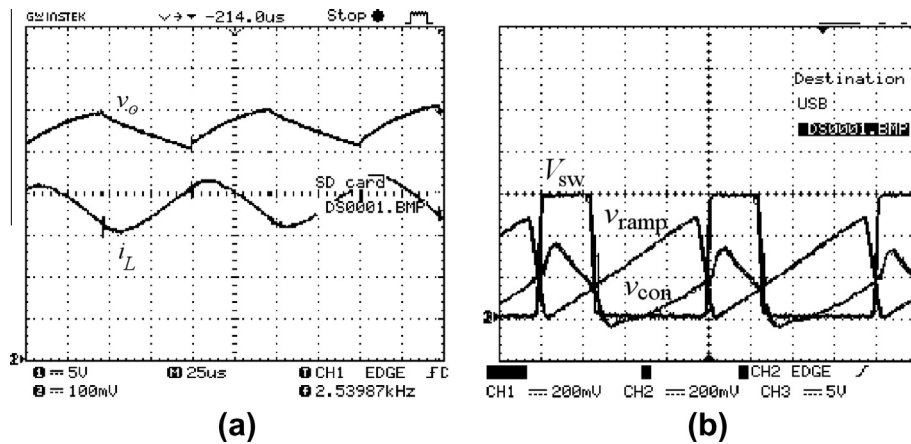
Fig. 26. MPPT control with $R = 140\ \Omega$ (a) inductor current (0.1 V/div) and the output voltage (5 V/div) (b) switch signal. Period-1 operation. The period of the waveforms is 100 μs.
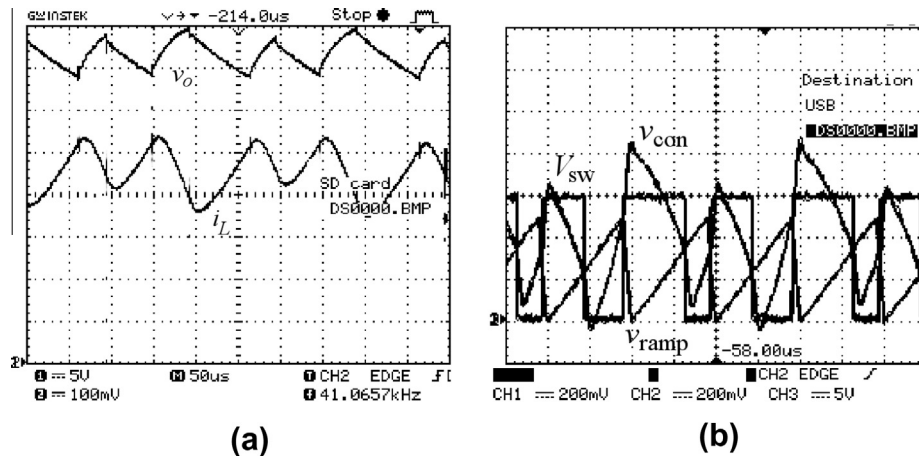
Fig. 27. MPPT control with $R = 180 \, \Omega$ (a) inductor current (0.1 V/div) and the output voltage (5 V/div) (b) switch signal. Period-2 operation. The period of the waveforms is 200 µs.

4.3. Maximum Power Point Tracking (MPPT) control

For $I_{ph} = 0.5$ A, the reference voltage is set at maximum power point $V_{ref} = 14.5$ V. The other parameters are fixed $K_p = 25$, $V_L = 0$ V, $V_U = 0.5$ V.

4.3.1. Varying load resistance

At lower values of the resistance the system is stable (Fig. 26). When the value of the reference current is increased, the system goes to period-doubling bifurcation as shown in Fig. 27.

5. Conclusion

In this paper we have considered the dynamical behavior of a boost converter fed from a photovoltaic panel. While most earlier works that study the nonlinear behavior of the combined system PV panel/DC–DC converter did not include the V–I properties of the PV panel, or the switched dynamics of the converter, in this work we thoroughly investigated these systems with numerical results that were analytically and experimental validated.

The conclusion drawn from the reported results are:

1. When the source is a photovoltaic panel instead of a voltage source, the v–i characteristics of the PV panel interacts with the nonlinear characteristics of the DC–DC converter, and, increases the range of stability of the converter.
2. We have investigated the phenomena in the commonly used controllers like the peak current mode controlled converter, average current mode controlled converter, voltage mode controlled converter, and a converter under maximum power point tracking control.
3. When a peak current mode controlled converter is used, the system becomes unstable for high values of the reference current (which becomes necessary for MPP tracking at high insolation). In the I_{ph}- I_{ref} parameter space, there is a definite region of

stability, and the controller has to be set to operate within that range. Similarly, the system may be destabilized for high values of the load resistance, and for every value of incident solar radiation, this critical value has been determined.

4. For average current mode control, the parameters of interest are I_{ph}, I_{ref}, R, and the controller gain K_p. Out of these, I_{ph} and R are uncontrolled parameters that depend on the solar radiation, and the load respectively. To achieve stable operation, the controlled parameters like I_{ref} and K_p should be set depending on the values of the uncontrolled variable parameters.
5. Since the prime objective of voltage mode control is to regulate the output voltage, this control cannot at the same time track the maximum power point. This problem can be overcome in the MPP tracking control, at the expense of a tight voltage regulation, and can extract a maximum amount of power from the PV panel. We showed that such a system can also lose stability for high values of the photo-current and load resistance.
6. For all the cases we have obtained the range of stability in the parameter space, which will help designers to set the parameters of the converter for use with photovoltaic source. The results have been obtained for a specific choice of the PV panel and converter parameters, but will be qualitatively true for systems with a different set of parameters. Our results have been validated through experimental investigation, whose parameters were different from that used in simulation.

References

Abouobaida, H., Cherkaoui, M., 2011. Robust controller for interleaved DC–DC converters and buck inverter in grid-connected photovoltaic systems. WSEAS Transactions on Power Systems 6 (1), 21–30.

Agrawal, S., 2012. Comparative Analysis of Hybrid Photovoltaic Thermal Air Collectors: Design, Modeling and Experiment to Improve the Overall Efficiency of PV System. LAP LAMBERT Academic Publishing.

Banerjee, S., Verghese, G.C., 2001. Nonlinear Phenomena in Power Electronics – Attractors, Bifurcations, Chaos, and Nonlinear Control. IEEE Press, New York.

Battisti, R., Corrado, A., 2005. Evaluation of technical improvements of photovoltaic systems through life cycle assessment methodology. Solar Energy 30 (7), 952–967.

Bennett, T., Zilouchian, A., Messenger, R., 2012. Photovoltaic model and converter topology considerations for MPPT purposes. Solar Energy 86 (7), 2029–2040.

Bull, S.R., 2001. Renewable energy today and tomorrow. Proceedings of the IEEE 89 (8), 1216–1226.

Chan, W.C.Y., Tse, C.K., 1997. Study of bifurcations in current-programmed DC/DC boost converters: from quasiperiodicity to period-doubling. IEEE Transactions on Circuits and Systems-I 44 (12), 1129–1142.

Deane, J.H.B., 1992. Chaos in a current-mode controlled boost DC–DC converter. IEEE Transactions on Circuits and Systems-I 39 (8), 680–683.

Enrique, J.M., Durán, E., de Cardona, M.S., jar, J.M.A., 2007. Theoretical assessment of the maximum power point tracking efficiency of photovoltaic facilities with different converter topologies. Solar Energy 81 (1), 31–38.

Esram, T., Chapman, P.L., 2007. Comparison of photovoltaic array maximum power point tracking techniques. IEEE Transactions on Energy Conversion 22 (2), 439–449.

Farahat, M.A., Metwally, H.M.B., Mohamed, A.A.-E., 2012. Optimal choice and design of different topologies of DC–DC converter used in PV systems, at different climatic conditions in Egypt. Renewable Energy 43, 393–402.

Giaouris, D., Banerjee, S., Zahawi, B., Pickert, V., 2008. Stability analysis of the continuous conduction mode buck converter via Filippov's method. IEEE Transactions on Circuits Systems-I 55 (4), 1084–1096.

Hohm, D.P., Ropp, M.E., 2003. Comparative study of maximum power point tracking algorithms. Progress in Photovoltaics: Research and Applications 11 (1), 47–62.

Jain, S., Agarwal, V., 2007. A single-stage grid connected inverter topology for solar PV systems with maximum power point tracking. IEEE Transactions on Power Electronics 22 (5), 1928–1940.

Kalirasu, A., Dash, S.S., 2010. Simulation of closed loop controlled boost converter for solar installation. Serbian Journal of Electrical Engineering 7 (1), 121–130.

Liu, Y.-H., Huang, J.-W., 2011. A fast and low cost analog maximum power point tracking method for low power photovoltaic systems. Solar Energy 85 (11), 2771–2780.

Maeda, T., Saito, T., 2010. Analysis of stability and bifurcation in a simple model of power converters with solar cell input. In: Proceedings of IEEE/IECON, Glendale, AZ, USA.

Morel, C., Petreus, D., Rusu, A., 2011. Application of the Filippov method for the stability analysis of a photovoltaic system. Advances in Electrical and Computer Engineering 11 (4), 93–98.

Salas, V., Olias, E., Barrado, A., Lazaro, A., 2006. Review of the maximum power point tracking algorithms for stand-alone photovoltaic systems. Solar Energy Materials and Solar Cells 90 (11), 1555–1578.

Siddiqui, M.U., Arif, A.F.M., Bilton, A.M., Dubowsky, S., Elshafei, M., 2013. An improved electric circuit model for photovoltaic modules based on sensitivity analysis. Solar Energy 90, 29–42.

Solangi, K.H., Islam, M.R., Saidur, R., Rahim, N.A., Fayaz, H., 2011. A review on global solar energy policy. Renewable and Sustainable Energy Reviews 15 (4), 2149–2163.

Suri, M., Huld, T.A., Dunlop, E.D., Ossenbrink, H.A., 2007. Potential of solar electricity generation in the European union member states and candidate countries. Solar Energy 81 (10), 1295–1305.

Taghvaee, M.H., Radzi, M.A.M., Moosavain, S.M., Hizam, H., Marhaban, M.H., 2012. A current and future study on non-isolated dcdc converters for photovoltaic applications. Renewable and Sustainable Energy Reviews 17, 216–227.

Tse, C.K., 2003. Complex Behavior of Switching Power Converters. CRC Press, New York.

Villalva, M.G., Gazoli, J.R., Filho, E.R., 2009. Comprehensive approach to modeling and simulation of photovoltaic arrays. IEEE Transactions on Power Electronics 25 (5), 1198–1208.

Wujian, Z., Qiuhua, L., 2008. Survey of maximum power point tracking techniques for photovoltaic array. High Voltage Engineering 34 (6), 1145–1154.

Xiao, W., Ozog, N., Dunford, W.G., 2007. Topology study of photovoltaic interface for maximum power point tracking. IEEE Transactions on Industrial Electronics 54 (3), 1696–1704.

Xiong, X., Tse, C.K., Ruan, X., 2012. Bifurcation in standalone photovoltaic-battery hybrid power systems. In: IEEE International Symposium on Circuits and Systems, Seoul, South Korea.

Xiong, X., Tse, C.K., Ruan, X., 2013. Bifurcation in standalone photovoltaic-battery hybrid power system. IEEE Transactions on Circuits and Systems-I 60 (5), 1354–1365.

Zegaoui, A., Aillerie, M., Petit, P., Sawicki, J.P., Charles, J.P., Belarbi, A., 2011. Dynamic behaviour of PV generator trackers under irradiation and temperature changes. Solar Energy 85 (11), 2953–2964.